ON THE COMPUTATION OF THE VELOCITY FIELD AND MASS BALANCE IN THE FINITE-ELEMENT MODELING OF GROUNDWATER FLOW

CONF-801217--2

Gour-Tsyh Yeh

Environmental Sciences Division
Oak Ridge National Laboratory
Oak Ridge, Tennessee 37830

ABSTRACT

Darcian velocity has been conventionally calculated in the finite-element modeling of groundwater flow by taking the derivatives of the computed pressure field. This results in discontinuities in the velocity field at nodal points and element boundaries. Discontinuities become enormous when the computed pressure field is far from a linear distribution. It is proposed in this paper that the finite element procedure that is used to simulate the pressure field or the moisture content field also be applied to Darcy's law with the derivatives of the computed pressure field as the load function. The problem of discontinuity is then eliminated, and the error of mass balance over the region of interest is much reduced. The reduction is from 23.8 to 2.2% by one numerical scheme and from 29.7 to -3.6% by another for a transient problem.

INTRODUCTION

To study the transport of dissolved constituents in a subsurface flow system, the velocity field therein must be determined first. Several finite-element Galerkin models have been developed to obtain the flow field [1-8]. The continuity equation of water-mass governing the distribution of pressure head was solved by the Galerkin finite-element method, subject to appropriate boundary and initial conditions. The flow field was computed with Darcy's law by taking the derivatives of the calculated pressure field [3-6]. Inherent in that approach, however, was the resulting discontinuity in the velocity at nodal points and element boundaries, which unfortunately lead to a violation of the conservation of mass in a local sense. Results from two hypothetical sample problems showed that the discontinuity in the velocity field obtained by the conventional approach ranges from very small to several hundred percent depending on the location in the region. Furthermore, the overall mass balance is not preserved. When spatial distribution of the velocity is significant, inputting this discontinuous flow field to the contaminant transport computation could conceivably produce large error.

It is proposed to solve Darcy's law for the velocity field at nodal points by the same finite-element method used for the pressure field rather than simply to take the derivatives of the approximate pressure field. This approach is consistent with the spirit of finite-element modeling of groundwater flow. It also yields a continuous velocity field over the region of interest including nodal points and element boundaries. Accordingly, this paper describes the use of the finite-element method, as applied to Darcy's law, to remove the discontinuity described above. The two hypothetical problems are reexamined in the light of the proposed approach, and the results are presented.

MATHEMATICAL STATEMENT

The governing equations to describe the water movement in variably saturated-unsaturated porous media have been derived in detail [4] in the following form:

$$F \frac{\partial h}{\partial t} - \partial_i [K_{ij} \partial_j H] - Q = 0 \tag{1}$$

and

$$V_i = -K_{ij} \partial_j H \quad , \tag{2}$$

where

$$F = \frac{\theta}{n} \alpha' + \beta' + \frac{d\theta}{dh} \tag{3}$$

and

$$H = h + z \quad , \tag{4}$$

in which h is the pressure head, θ is the moisture content, n is the effective porosity, α' and β' are the modified coefficients of compressibility of the medium frame and water, respectively, K_{ij} is the hydraulic conductivity tensor, V_i is the Darcian velocity vector, t is the time, Q is the artificial recharge or withdrawal, z is vertical coordinate, and H is the total head. In Eqs. (1) and (2),

∂_i denotes the partial differentiation with respect to the spatial coordinate, x_i; and $z = x_3$ is the vertical coordinate. In general, Eq. (1) is nonlinear because both the soil property, F (represented by Eq. (3)), and hydraulic conductivity tensor, K_{ij}, are nonlinear functions of the pressure head, h.

The initial condition of Eq. (1) may take the following form:

$$h = h_o(x_i) \qquad \text{in} \quad R \ , \tag{5}$$

where h_o is a prescribed function of the spatial coordinate, x_i, R is the region of interest enclosed by the boundary, $B(x_1, x_2, x_3) = 0$ as shown in Fig. 1. The function, h_o, may also be obtained by simulating the steady-state version of Eq. (1) with time-invariant boundary conditions. In the groundwater flow model, three types of boundary conditions are generally encountered. On the first type (Dirichlet) boundary, the pressure head is prescribed:

$$h = h_1(x_i, t) \qquad \text{on} \quad B_1 \ , \tag{6}$$

where B_1 is a portion of the boundary B and h_1 is a given input function of time and spatial coordinate on B_1. On the second type (Neumann) boundary, the flux is prescribed as:

$$- n_i \cdot K_{ij} \cdot \partial_j H = q_2 \qquad \text{on} \quad B_2 \ , \tag{7}$$

where n_i is the directional cosine of the outward unit vector normal to the B_2 portion of the boundary B. The third type is the variable boundary in the sense that either the Dirichlet or the Neumann conditions may prevail:

$$h = h_3(x_i, t) \qquad \text{on} \quad B_3 \tag{8a}$$

or

$$- n_i \cdot K_{ij} \cdot \partial_j H = q_3 \qquad \text{on} \quad B_3 \ , \tag{8b}$$

where h_3 and q_3 are two known input functions of time and spatial coordinate x_i on the B_3 portion of B. The boundaries, B_1, B_2, B_3, and the impervious boundary, B_I, constitute the entire boundary, $B(x_1, x_2, x_3) = 0$. Initially Eq. (8a) is applied to the boundary B_3 when the exact boundary conditions cannot in general be predicted a priori. Such a case would arise at the ground surface where either ponding (Dirichlet) or infiltration (Neumann) conditions could prevail [6]. This can only be determined in the cyclic process of solving Eqs. (1) and (2).

Applying the Galerkin finite-element procedure to Eq. (1), one obtains the following matrix equation:

$$[M_{ij}]\{\dot{h}_j\} + [S_{ij}]\{h_j\} + \{D_i\} + \{Q_i\} = 0 \quad , \tag{9}$$

where the temporal derivative of the head, h_j is given by

$$\dot{h}_j = \frac{dh_j}{dt} \quad . \tag{10}$$

The matrix equation coefficients are defined as:

$$M_{ij} = \int_R N_i F N_j \, dR \quad , \tag{11}$$

$$S_{ij} = \int_R \{(\partial_m N_i)\cdot K_{mn}\cdot(\partial_n N_j)\} dR \quad , \tag{12}$$

$$D_i = \int_R [K_{m3}\cdot(\partial_m N_i) - Q N_i] \, dR, \quad \text{and} \tag{13}$$

$$Q_i = \int_{B_2} N_i q_2 \, dB + \int_{B_3} N_i q_3 \, dB \quad , \tag{14}$$

where N_i is the basis function at the nodal point i.

Eq. (9) can be solved by any of the six alternative numerical schemes listed in Table 1 [8]. They are dependent on the method of time marching and the treatment of the mass matrix, $[M_{ij}]$. For example, scheme 1 uses the central difference time marching with no mass lumping for the matrix, $[M_{ij}]$.

After the pressure field, h, is obtained, the Darcian velocity can be obtained by Darcy's law, Eq. (2). Conventionally, it is evaluated numerically by taking the derivative of the approximate pressure field, $h = h_k N_k$, as follows:

$$V_i = -K_{ij} [\partial_j (h_k N_k) + \delta_{j3}] \quad . \tag{15}$$

This approach naturally yields the discontinuity in the velocity, V_i, at nodal points and element boundaries. If continuity is to be achieved, the nodal gradient must also be treated as an unknown [6]. This in turn will increase, by a factor of 3 in the two-dimensional problems or 4 in the three-dimensional problems, the number of equations and the bandwidth of the system and thereby increase drastically the computing time and computer storage requirements. To circumvent this problem, it is proposed that the finite-element method be applied to Eq. (2) to yield:

$$[S'_{ij}]\{V_{nj}\} = \{D_{ni}\} \qquad n = 1, 2, \text{ or } 3 \quad , \tag{16}$$

where

$$S'_{ij} = \int_R N_i N_j \, dR \tag{17a}$$

and

$$D_{ni} = - \int_R N_i [K_{nm} \{\partial_m (N_j h_j) + \delta_{m3}\}] \, dR \tag{17b}$$

Eqs. (9) and (16) can be solved simultaneously by iteration. This will not complicate the problem, since Eq. (9) has to be solved iteratively because of its nonlinearity for each time step. It will not require any additional storage either. However, it will increase the CPU time by a factor of less than 3 or 4 for two- and three-dimensional problems respectively. If the storage for the matrix $[S'_{ij}]$ is available, the CPU time will remain practically the same as the conventional approach, because $[S_{ij}]$ needs to be evaluated and triangularized only once.

The mass balance over the whole region of interest is obtained by integrating Eq. (1):

$$\int_R F \frac{\partial h}{\partial t} \, dR = \int_B F_n \, dB \quad , \tag{18}$$

where F_n is the normal flux through the global boundary $B(x,z) = 0$. In fact, F_n denotes:

$$F_n = n_i \, K_{ij} \, \partial_j H \quad . \tag{19}$$

Having obtained the pressure head field, h, one could integrate the rightand left-hand sides of Eq. (18) independently. If the solution for h is free of error, one would expect the equality of the two integrals. In this paper, the integral of the right-hand side is broken into five components:

$$F_D = \int_{B_1} F_n \, dB \quad , \tag{20}$$

$$F_N = \int_{B_2} F_n \, dB \quad , \tag{21}$$

$$F_S = \int_{B_{3S}} F_n \, dB \quad , \tag{22}$$

$$F_R = \int_{B_{3R}} F_n \, dB \quad , \text{ and} \tag{23}$$

$$F_I = \int_{B_I} F_n \, dB \quad , \tag{24}$$

where F_D, F_N, F_S, F_R, and F_I represent the fluxes through the Dirichlet boundary, B_1; the Neumann boundary, B_2; the seepage boundary, B_{3S}; the rainfall-infiltration boundary, B_{3R}; and the impervious Neumann boundary, B_I; respectively. On the other hand, the integral on the left-hand side of Eq. 18,

$$F_V = \int_R F \frac{\partial h}{\partial t} dR \quad , \tag{25}$$

represents the volumetric increasing rate of the moisture content in the region. For exact solution, the net flux across the whole boundary, defined by

$$F_{net} = F_D + F_N + F_S + F_R + F_I \tag{26}$$

should satisfy the following equation:

$$F_{net} = F_V \quad . \tag{27}$$

In addition, F_I should theoretically be equal to zero. However, in any practical numerical simulation, Eq. (27) will not be satisfied and F_I will be nonzero. Nevertheless, the mass balance computation should provide a means to check the numerical scheme and consistency in the computer code.

RESULTS

Two sample problems are used to compare the results from the models represented by Eqs. (15) and (16), respectively. The first example is a hypothetical seepage pond problem described earlier [9]. The second one is the Freeze's transient problem reported elsewhere [4,10]. In addition, results by all six alternative numerical schemes (Table 1) are compared in both examples.

Seepage Pond Problems

A seepage pond is assumed to be situated entirely in the unsaturated zone above a water table (Fig. 2a). This pond provides a source

of water which infiltrates into subsurface aquifers. After water reaches the water table, it flows toward a stream. Is is further assumed that the system is composed of highly permeable sand with soil properties shown in Fig. 3. For the finite-element computation, the entire region is discretized by 595 nodal points and 528 elements (Fig. 2b). Seven nodal points on the stream-soil interface are designated as Dirichlet nodes. Seven nodal points on the bottom of the seepage pond are considered as constant Neumann flux points and are assigned a constant infiltration rate of 4.0×10^{-4} cm/s. The top sides of all elements on the sloping surface, except the two elements immediately to the right of the seepage pond, are considered variable boundary surface, i.e., seepage-rainfall boundary. In other words, the nodal points on this surface are either Dirichlet or Neumann points with the infiltration rate equal to the excess rainfall rate.

The Darcian velocity field computed by model Eq. (15) shows the discontinuity at every nodal point as indicated by multivectors at any point in Fig. 4. The severity of this discontinuity depends on the location. This discontinuity is completely eliminated with model Eq. (16) as can be seen from Fig. 5, which shows the unique velocity vector at all nodal points. Table 2 shows the comparison of the computed Darcian velocity components simulated by model Eq. (15) and (16), respectively, for the three selective nodal points 2, 179 and 587 (Fig. 2). These three sample points are taken from computer output to illustrate the difference between the two models. It is seen that at nodal point no. 2, the vertical velocity component as computed from element no. 2 is about 2.58 times that computed from element no. 1. The values of the horizontal component, V_x, at nodal point no. 179 as computed from element nos. 159 and 160 are about 1.41 times those computed from element nos. 152 and 153; while the values of the vertical component, V_z, at the same point as computed from element nos. 153 and 160 are about 4.69 times those computed from element nos. 152 and 159. At nodal point no. 587, the vertical velocity component, V_z, as computed from element no. 522 is about 1.27 times that computed from element nos. 521 and 528. On the other hand, results from model Eq. (15) show that the values of velocity components are identical at the same point as is expected. However, the CPU times on IBM 360/91 by model Eq. (15) and (16) are 0.92 and 2.51 minutes, respectively. A saving of computer storage of about 150 K is achieved by model Eq. (16) though. Since the steady-state solution is sought, numerical scheme nos. 1 through 6 (Table 1) yield identical results as expected.

Freeze Transient Problem

A very small (6 x 3 m) laboratory-sized watershed was monitored by Freeze [10] to test his finite difference computer code. The same data were also used by Reeves and Duguid [4] to debug and test their finite-element model. These watershed data are again used in the present paper to compare model Eqs. (15) with (16).

The flow system is shown in Fig. 6. It is composed of highly permeable sand, the unsaturated properties of which are shown in Fig. 3. To obtain initial conditions, pressure-head values were pre- scribed along the stream channel, part of the slope, and the upper plateau. Taking all other boundaries to be impermeable, a steady-state solution was determined which was the initial condition for the transient calculation.

Using Freeze's transient boundary condition (Figure 6b) and Reeves and Duguid's finite-element discretization #2 (Figure 6c), results obtained by models Eqs. (15) and (16), respectively, are shown in Figs. 7 and 8. Model Eq. (15) again displays the discontinuity of velocity vectors at all nodal points, while model Eq. (16) has completely eliminated this inconsistency. Furthermore, Table 3 shows that the mass balance has not been satisfied by model Eq. (15). At the end of about 3-h simulation time, the total net mass through all boundaries is only about 76.2% of the mass accumulated in the media as computed by numerical scheme no. 1 of model Eq. (15). In other words, 23.8% of the mass has not been accounted for, i.e., has been lost through boundaries. Reeves and Duguid [4] speculated that this large loss of mass might be eliminated by adding triangular elements. However, without using triangular elements, model Eq. (16) only yields a 2.2% mass loss by eliminating the discontinuity of the velocity and using Eq. (25) to evaluate the moisture rate change. An even larger mass loss of 29.7% is obtained by numerical scheme no. 2 of model Eq. (15). Model Eq. (16), on the other hand, renders a 3.6% mass gain. Thus, error of mass balance (positive for loss, negative for gain) by model Eq. (16) is much smaller than that by model Eq. (15). The CUP time on IBM 360/91 for models Eq. (15) and Eq. (16) are 2.3 and 4.5 minutes, respectively, but a saving of computer storage of about 140 K is obtained by the latter.

Table 3 also shows the percentage of mass change by all alternative numerical schemes. It is noted that the central difference standard Galerkin scheme in model Eq. (16) yields the best results. This is not surprising since the water transport equation does not contain advection terms.

CONCLUSION

A continuous velocity field is required for the simulation of waste transport in the subsurface aquifer system. The conventional approach used in finite-element modeling, that is, taking the derivative of the approximately computed pressure head field, results in discontinuity of velocity at element boundaries and nodal points. It may also yield large error in overall mass balance computation. Thus, it is imperative that the same finite-element method that is employed to simulate the pressure field be applied to Darcy's law to obtain the velocity field. This will ensure a continuous velocity field and greatly reduce the overall mass balance error. The central difference Galerkin scheme yields the lowest error, since the governing equation is basically the Laplacian type in spatial coordinates.

REFERENCES

1. S. P. Neumann and P. A. Witherspoon, "Analysis of nonsteady flow with a free surface using the finite element method," Water Resour. Res., 7(3), 611-623 (1971).

2. G. F. Pinder and E. O. Frind, "Application of Galerkin procedure to aquifer analysis, Water Resour. Res., 8(1), 108-120 (1972).

3. G. F. Pinder, "A galerkin finite element simulation of groundwater contamination on Long Island, New York," Water Resour. Res., 9(6), 1657-1669 (1973).

4. M. Reeves and J. O. Duguid, Water Movement Through Saturated-Unsaturated Porous Media: A Finite Element Galerkin Model, ORNL-4927, Oak Ridge National Laboratory, Oak Ridge, Tennessee (1975).

5. S. K. Gupta, K. K. Tanji, and J. N. Luthin, A Three-dimensional Finite Element Groundwater Model, University of California, Davis, Water Resources Center Contribution Series #152 (1975).

6. G. Segol, A Three-dimensional Galerkin Finite-Element Model for the Analysis of Contaminant Transport in Variably Saturated-Unsaturated Porous Media, Dept. of Earth Sciences, University of Waterloo, Canada (1976).

7. Y. H. Huang and S. J. Wu, "Comparison of Three-dimensional Finite Elements for Aquifer Simulation, Finite Element in Water Resources," Proceedings of the First International Conference on Finite Elements in Water Resources, edited by W. G. Gray, G. F. Pinder and C. A. Brebbia, Pentech Press, London, pp. 2.87-2.105 (1977).

8. G. T. Yeh and D. S. Ward, FEMWATER: A Finite Element Model of Water Flow through Saturated-Unsaturated Porous Media, ORNL-5567, Oak Ridge National Laboratory, Oak Ridge, Tennessee (1980).

9. J. Duguid and M. Reeves, Material Transport in Porous Media: A Finite Element Galerkin Model, ORNL-4928, Oak Ridge National Laboratory, Oak Ridge, Tennessee (1976).

10. R. A. Freeze, A Physics-based Approach to Hydrologic Response Modeling: Phase I - Model Development, Completion Report for OWRR Contract No. 14-31-001-3604, Dept. of the Interior, Washington, D.C. (1972).

Table 1. Listing of Alternative Numerical Schemes

Numerical schemes	Time-marching			Mass matrix	
	Central difference	Backward difference	Mid-difference	Without lumping	With lumping
1	X			X	
2		X		X	
3	X				X
4		X			X
5			X	X	
6			X		X

Table 2. Comparison of Velocity (cm/sec) Components Simulated by Model Eqs. (15) and (16), Respectively, at Three Selected Points

Node number	Element number	Model Eq. (15)		Model Eq. (16)	
		V_x	V_z	V_x	V_z
2	1	2.38E-8	-2.253E-8	1.24E-8	-4.44E-8
	2	2.33E-8	-6.54E-8	1.24E-8	-4.44E-8
179	152	2.26E-5	-9.15E-5	3.03E-5	-2.94E-4
	153	2.26E-5	-4.31E-4	3.03E-5	-2.94E-4
	159	3.31E-5	-9.15E-5	3.03E-5	-2.94E-4
	160	3.31E-5	-4.31E-4	3.03E-5	-2.94E-4
587	521	6.28E-5	1.85E-4	1.23E-5	1.84E-4
	522	6.28E-5	2.36E-4	1.23E-5	1.84E-4
	528	7.89E-10	1.85E-4	1.23E-5	1.84E-4

Table 3. Comparison of Percentage of Mass Change of Freeze's Transient Problem as Simulated by Model Eq. (15) and (16)

	Scheme					
Model	1	2	3	4	5	6
Eq. (15)	23.8	29.7	N/A	N/A	N/A	N/A
Eq. (16)	2.2	-3.6	8.9	3.0	-3.2	-3.3

FIGURE LIST

Caption

Fig. 1. Spatial boundaries, B_1, B_2, B_3, and B_1, of flow region R. (B.C. = Boundary Conditions).

Fig. 2. Spatial discretization of the seepage pond problem.

Fig. 3. Hydraulic conductivity and soil moisture characteristics of a hypothetical sandy soil.

Fig. 4. Flow velocity plot as simulated by model Eq. (15) for the seepage pond problem.

Fig. 5. Flow velocity plot as simulated by Model Eq. (16) for the seepage pond problem.

Fig. 6. Configuration of Freeze's experimental watershed: (a) steady state boundary condition, (b) transient boundary condition, (c) spatial finite element discretization after Reeves and Duguid (1975).

Fig. 7. Flow velocity plot at time equal to 2.96 h of Freeze's transient problem as simulated by Model Eq. (15).

Fig. 8. Flow velocity plot at time equal to 2.96 h of Freeze's transient problem as simulated by Model Eq. (16).

ORNL-DWG 78-20110R

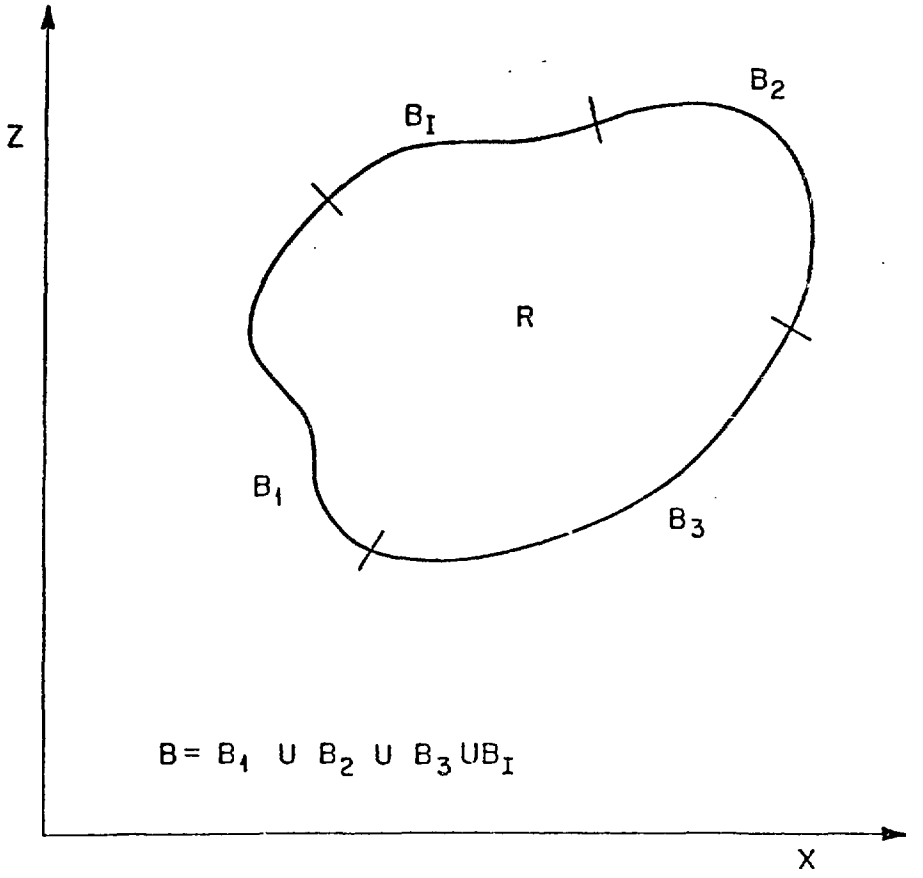

Fig. 1

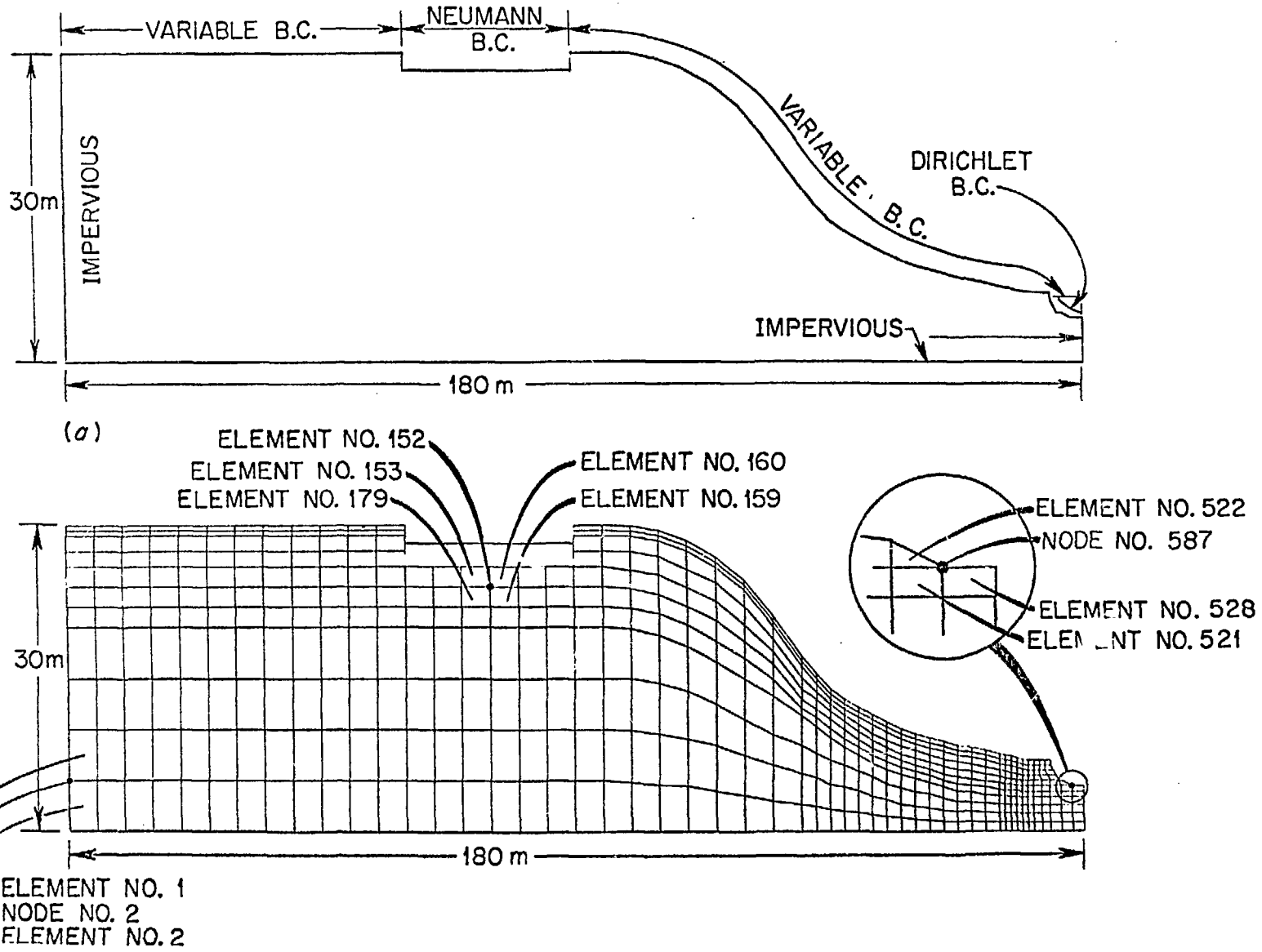
VARIABLE B.C.
NEUMANN B.C.
VARIABLE B.C.
DIRICHLET B.C.
IMPERVIOUS
30m
IMPERVIOUS
180 m
(a)
ELEMENT NO. 152
ELEMENT NO. 153
ELEMENT NO. 179
ELEMENT NO. 160
ELEMENT NO. 159
ELEMENT NO. 522
NODE NO. 587
ELEMENT NO. 528
ELEMENT NO. 521
30m
180 m
ELEMENT NO. 1
NODE NO. 2
ELEMENT NO. 2

Fig. 2

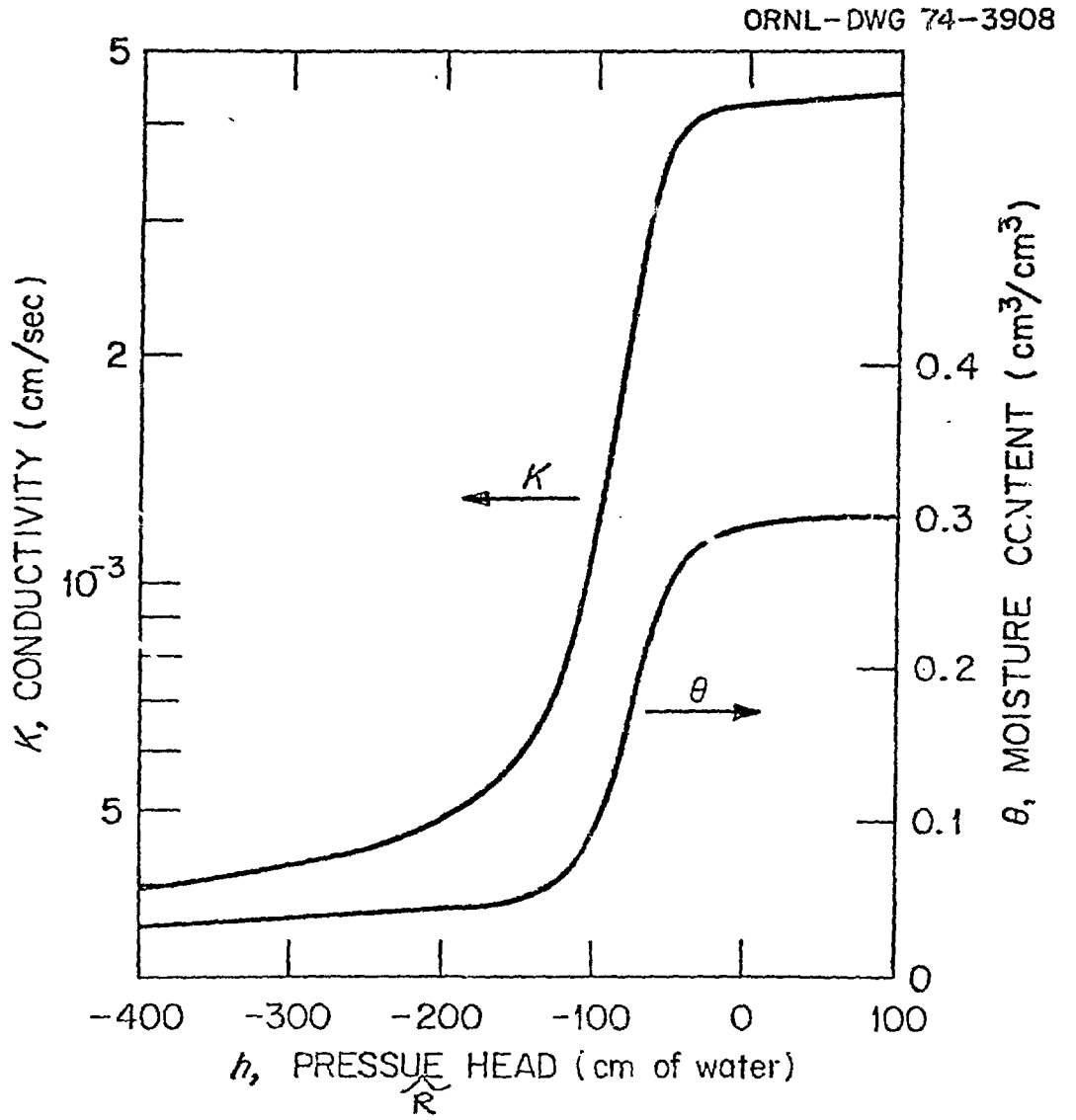
ORNL-DWG 74-3908
5
2
10^{-3}
5
K, CONDUCTIVITY (cm/sec)
K
θ
0.4
0.3
0.2
0.1
0
θ, MOISTURE CONTENT (cm³/cm³)
-400
-300
-200
-100
0
100
h, PRESSURE HEAD (cm of water)

Fig. 3

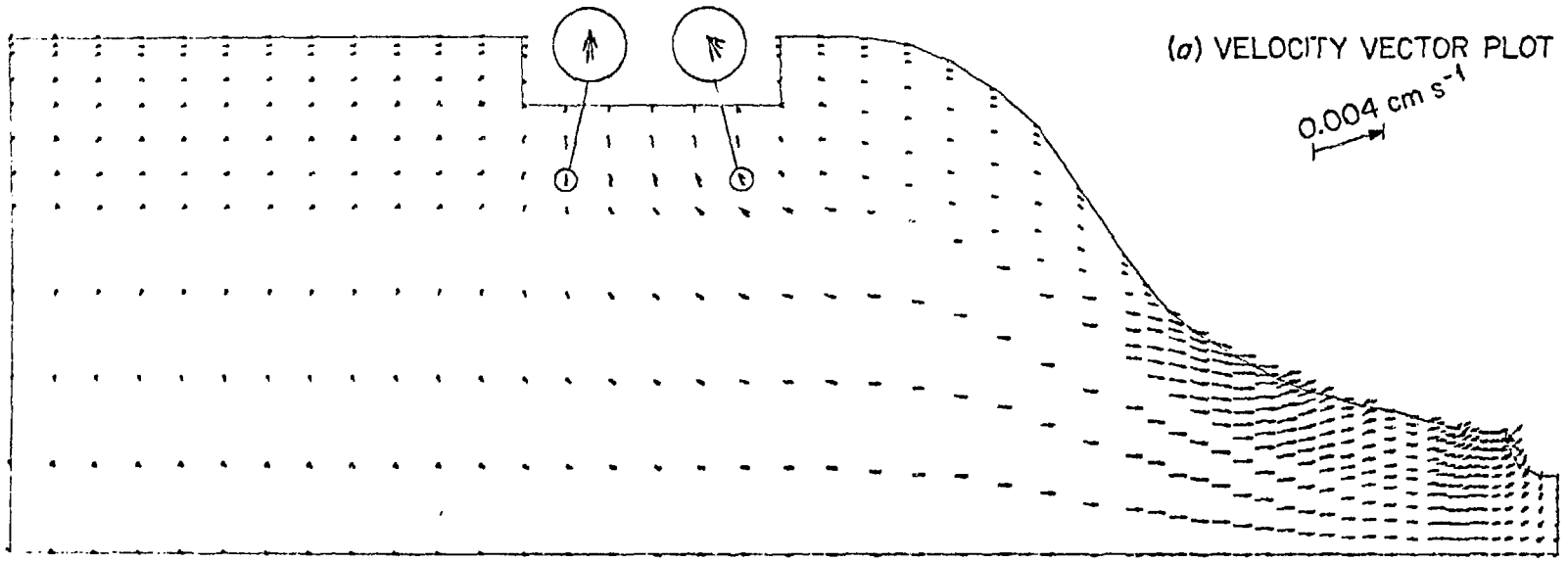

Fig. 4

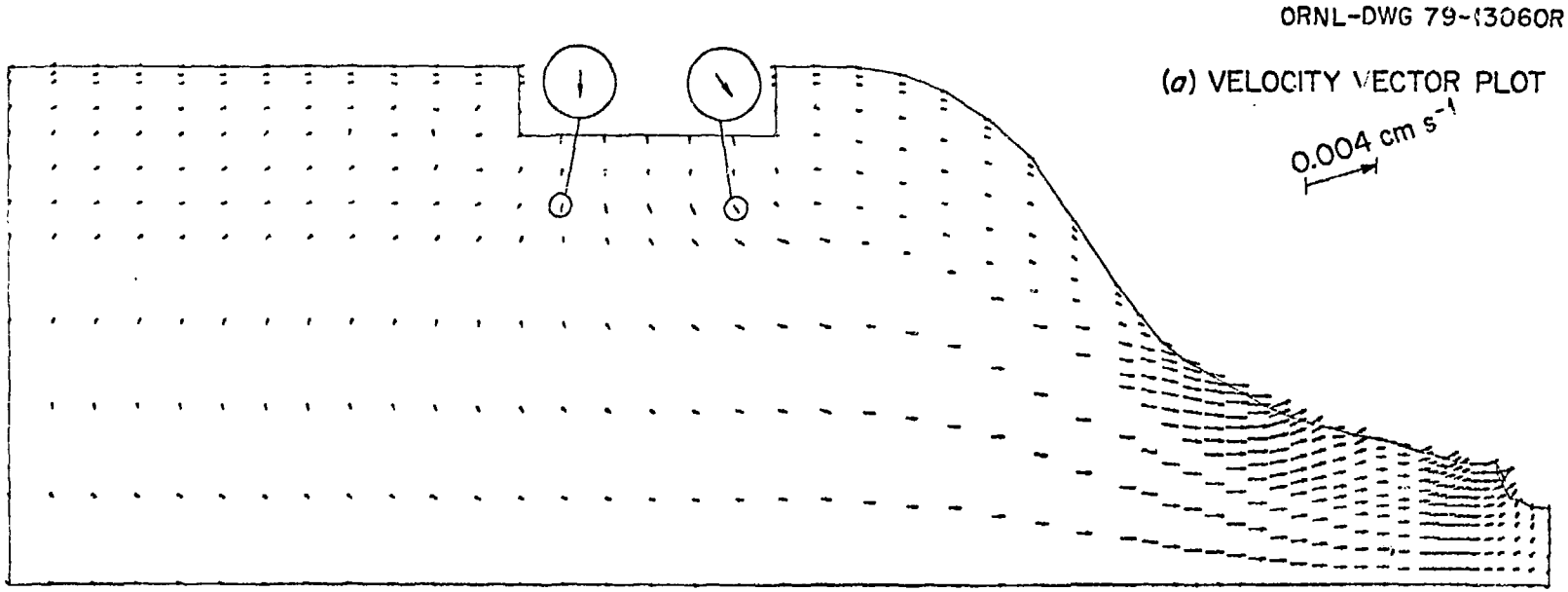

Fig. 5

ORNL-DWG 79-13083R

• Comparison with FD Solution

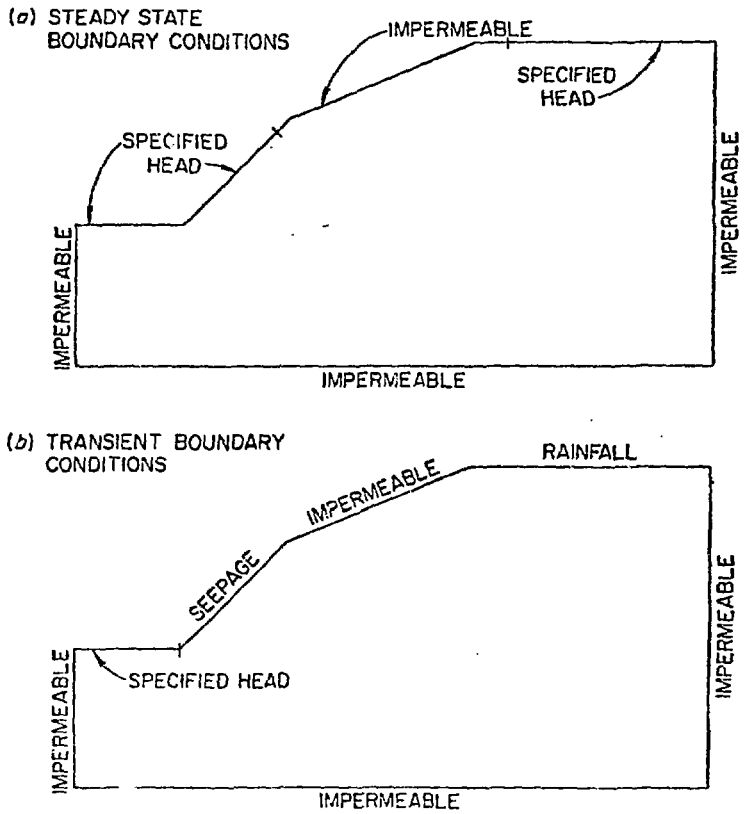

Fig. 6

ORNL-DWG 79-13082R

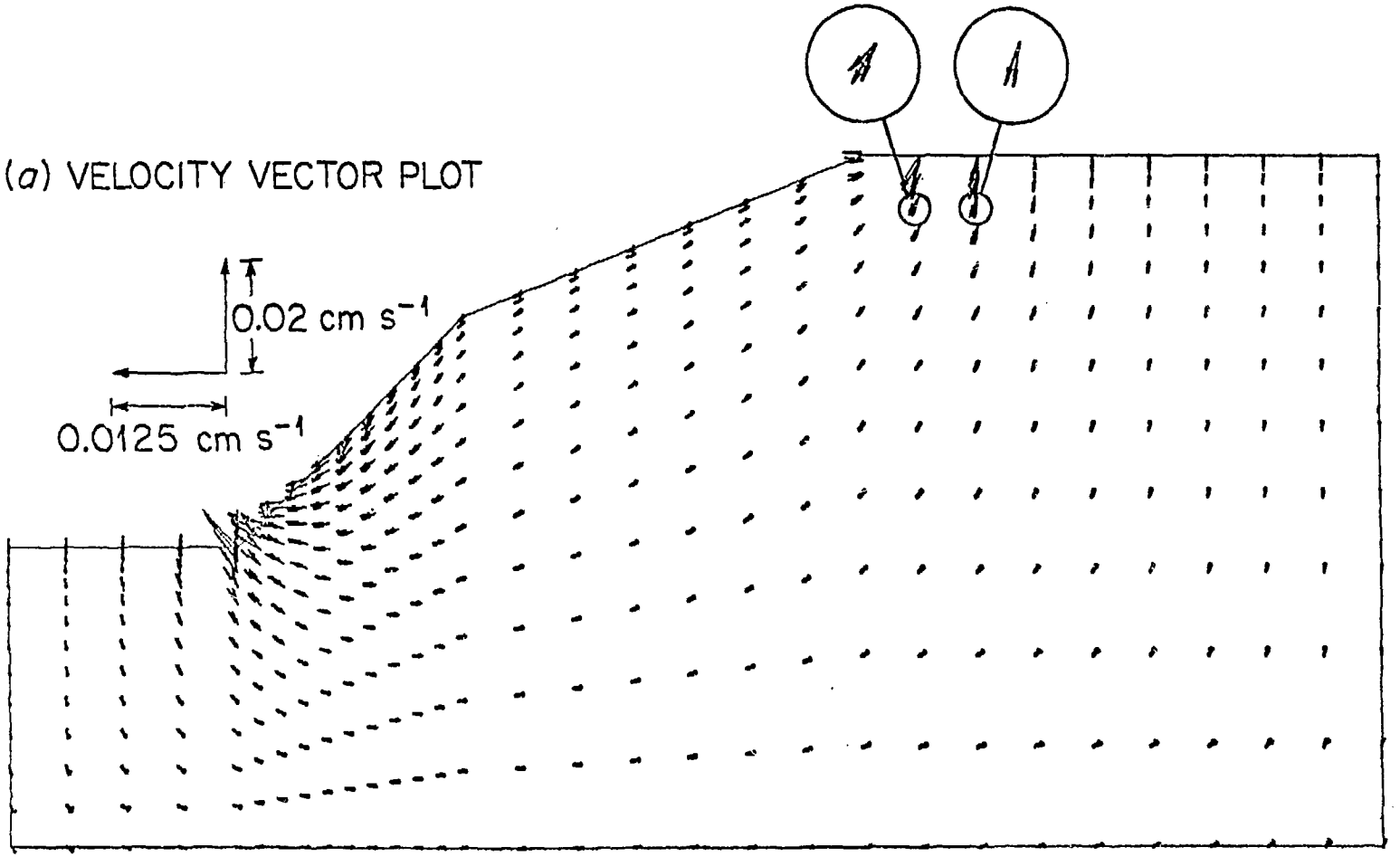

Fig. 7

ORNL-DWG 79-13067R

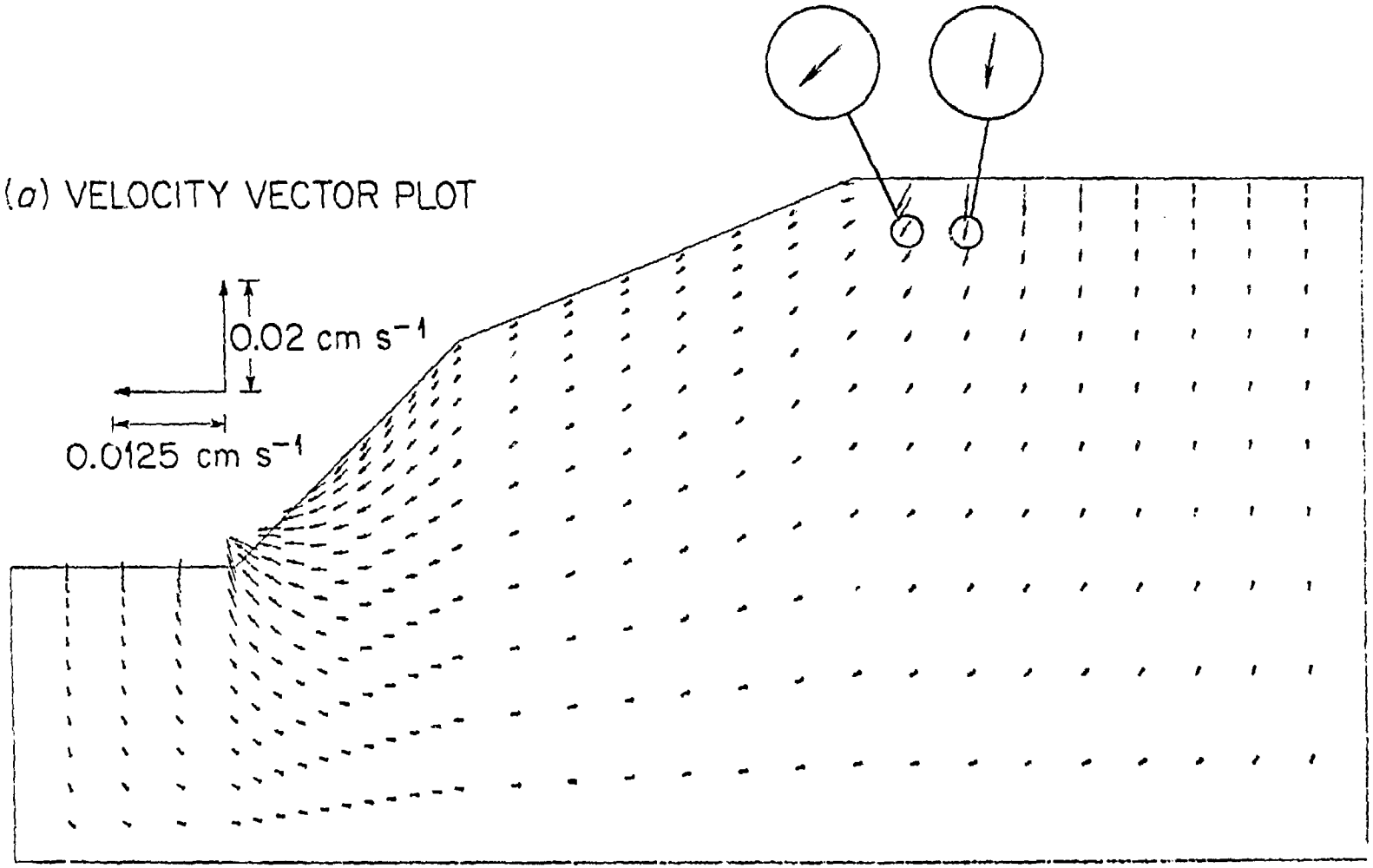

Fig. 8